Journal of Materials Processing Technology 211 (2011) 1400–1408

Contents lists available at ScienceDirect

Journal of Materials Processing Technology

journal homepage: www.elsevier.com/locate/jmatprotec

Evaluation of titanium alloy fabricated using electron beam melting system for dental applications

Mari Koike[a,*], Kelly Martinez[a], Lilly Guo[a], Gilbert Chahine[b], Radovan Kovacevic[b], Toru Okabe[a]

[a] Department of Biomaterials Science, Baylor College of Dentistry, Texas A&M Health Science Center, 3302 Gaston Ave., Dallas, TX 75246, USA
[b] Research Center for Advanced Manufacturing, Department of Mechanical Engineering, Southern Methodist University, 3101 Dyer Street, Dallas, TX 75205, USA

ARTICLE INFO

Article history:
Received 24 November 2010
Received in revised form 28 February 2011
Accepted 13 March 2011
Available online 21 March 2011

Keywords:
Rapid prototyping
Titanium alloy
Mechanical properties
Grindability
Corrosion behavior
Dental applications

ABSTRACT

In recently advanced rapid prototyping and manufacturing methods, one additional process is to use an electron beam to fabricate metal objects by the layer by layer sintering and/or melting metal powder. This method is often called electron beam melting (EBM). This study examined the mechanical properties, the grindability and corrosion resistance of Ti–6Al–4V ELI (extra low interstitial) specimens which were fabricated by the electron beam melting (EBM) process. Dumbbell-shaped specimens and two kinds of plate specimens were prepared using the Ti–6Al–4V ELI powder in the EBM system. The yield strength, tensile strength, modulus of elasticity and percent elongation at a crosshead speed of 0.25 mm/min were tested. The Vickers hardness in interior structures was determined. Grindability was evaluated as volume loss (mm^3) when the specimen was abraded using a SiC wheel at 1250 m/min for 1 min. Lastly, corrosion behavior was examined using the dynamic potentiostatic polarization technique in an artificial saliva at 37 °C. As controls, cast and commercial wrought alloys of Ti–6Al–4V ELI and commercially pure titanium (CP Ti) were evaluated. Cast specimens were prepared in a centrifugal casting machine using a MgO based mold. For the cast specimens, all the mechanical properties, grindability and corrosion characteristics were tested. On the other hand, for wrought specimens, only grindability and corrosion properties were tested. The yield and tensile strength of the as-fabricated Ti–6Al–4V ELI specimens without any additional metallurgical treatments were found to be 735 MPa and 775 MPa, respectively. The elongation was 2.3%. These values are well within many of precious and non-precious dental casting alloys.

1. Introduction

Anusavice (2003) describes that Tagart's presentation to the New York Odontological Group in 1907 on the fabrication of cast inlay restorations developed in 1905 has often been acknowledged as the first reported application of the lost-wax investment casting technique in dentistry. For many years, and still now, this lost-wax investment casting technique has been the main method of fabrication of various dental prostheses such as inlays, onlays, crowns, fixed bridges and frameworks for removable dentures. With continued improvements and development in casting techniques over the years, the present dental casting method has reached a point where cast prostheses not only satisfy the required accuracy, but also other requirements. Now, the method is not limited just to casting precious and non-precious dental casting alloys but expanded to make more biocompatible titanium alloys. A number of titanium alloys has successfully been cast with properties well comparable to those of traditional dental alloys (Koike et al., 2007). However, the dental lost-wax casting process consists of multiple steps and is extremely demanding.

In the new fields of solid free form fabrication, a process using a laser beam or electron beam as energy sources has been developed for sintering and/or melting the metal powder to build designed components. As Murr et al. (2009a) presented, this method is able to fabricate, under computer controls, intricate shapes of custom-designed parts and components. Cooper (2001) described that in this method, a laser or an electron beam scans on a layer of metal powder on a substrate, forming a melt pool and solidifying a fully dense layer with a fine scale of microstructure. Guided by a computer-aided design (CAD) model and computer control, each layer can result in a designed architecture. The building up of such layers can end up a complicated three-dimensional (3D) component that cannot be fabricated by traditional methods, such as metal casting or net-shape powder metallurgy. These solid form fabrication methods are often called the selective laser melting (SLM) process or the electron beam melting (EBM) process depending on the energy source they utilize (Christensen, 2007). Fundamentals, principles and their specific features of these processes have been reviewed in a number of publications. Lü et al. (2001), in their book on a rapid prototyping of the laser-

* Corresponding author. Tel.: +1 214 370 7005; fax: +1 214 370 7001.
E-mail address: mkoike@bcd.tamhsc.edu (M. Koike).

0924-0136/$ – see front matter © 2011 Elsevier B.V. All rights reserved.
doi:10.1016/j.jmatprotec.2011.03.013

induced technology, summarized findings in the 1990s regarding principles of the equipment and its commercial applications with different metals; Das (2003) reported physical aspects of SLM processing including oxidation, non-equilibrium wetting, epitaxial solidification, metal vaporization, etc.; and, again for the SLM method, Regenfuss et al. (2007) made the elucidation of certain mechanisms of laser material processing and, in particular, laser microsintering. On the other hand, for the EBM methods, Heinl et al. (2008) reviewed its processing mechanism and capability of fabrication of cellular titanium. With an increased feasibility of practical applications of both SLM and EBM process, various metal pieces and parts have been fabricated and evaluated, for example, as described in a book by Lü et al. (2001). These metals include some carbon steel, stainless steel and titanium. By claiming advantages of the EBM process, mainly the higher power density and beam velocity of the electron beam used in the system, Milberg and Sigl (2008) described physical effects and the measures in the EBM operation, reporting the results on a high-tensile steel powder.

The possibility of fabricating custom-designed parts using titanium alloys, which are known to be a troublesome metal in machining and casting, drew an attention to the medical and dental community. It would be very beneficial for medical and dental needs, if custom designed parts can be made more economic by using biocompatible titanium. Some of the trials using the SLM include an animal test of titanium dental implants (Tolochko et al., 2002); the effect of the processing parameters on the characteristics of titanium teeth models build (Santos et al., 2004); an attempt of making custom orthopedic implants (Harrysson, 2005); the properties examination of craniofacial scaffolds (Hollister et al., 2005), a trial of fabricating various detailed anatomic models for dental applications (Wehmöller et al., 2005), titanium dental implants with a porous surface structure to increase bone osseointegration and compact core to provide a desirable strength (Laoui et al., 2006), an experiment of fabricating a shape memory alloy, NiTi (Krishna et al., 2007); a possibility of manufacturing customized biomedical implant and surgical devices (Kotila et al., 2007); marginal fit of crowns made using dental alloys, Co–Cr and Au-Pt alloys (Quante et al., 2008); a designing bone in-growth structure using titanium for orthopedic applications (Mullen et al., 2009a, 2009b), designing and fabrication of porous medical prostheses using metals and alloys including Ti–6Al–4V (España et al., 2010), an in vivo study of Ti–6Al–4V implants (Mangano et al., 2010a,b), and a designing customized mandible prostheses and porous structures using Ti–6Al–4V (Bertol et al., 2010). On the other hand, the feasibility of fabricating biomedical devices using the EBM has been published. Some selected articles include titanium root-form implants (Ti–6Al–4V ELI) (Chahine et al., 2008), the femur-hip implants (Harrysson et al., 2008), Ti–6Al–4V cylindrical implants tested for early bone responses in rabbit (Thomsen et al., 2009), fabrication and strength characterization of porous Ti–6Al–4V structures (Li et al., 2009), in vivo performance of porous Ti–6Al–4V structures (Ponader et al., 2010), titanium (Ti–6Al–4V ELI) cylindrical implants placed in rabbits for the comparative in vivo performance with that of cast implants (Khouja et al., 2010a) and titanium (Ti–6Al–4V ELI) cylindrical implants which were compared with commercial implants for their in vivo performance (Khouja et al., 2010b). In addition, there is an investigation of in vitro biocompatibility of EBM-fabricated Ti–6Al–4V (Haslauer et al., 2010).

As described above, various applications of medical and dental prostheses made by SLM or EBM have been tried. One requisite for practical usages of these products is that the SLM and EBM components must satisfy required basic mechanical properties required for the applications. Thus, a number of groups of investigators examined strength characteristics of those products. The strengths of titanium specimens (Ti–6Al–4V) fabricated by SLM was reported as early as 1998 (Das et al., 1998). Their specimens seemed to be treated using HIP (hot isostatic pressing) and had a tensile strength higher than 1000 MPa. Also, before 2000, other researchers tested the mechanical properties of Ti–6Al–4V specimens made by SLM but the HIP process was necessary to obtain the strength comparable to the corresponding wrought alloys (Lü et al., 2001). Additionally, Levy et al. (2003) reported the strength of the SLM Ti–6Al–4V after the HIP treatment. In Santos et al. (2006), reviewed specifics of various laser forming systems and reported mechanical properties of metal component fabricated. In contrast to the SLM specimens, the evaluation of the mechanical properties of EBM titanium was reported more recently, since the EBM equipment became available in the last few years. Lindhe and Harrysson (2003) reported their initial trial of the EBM process for various alloys. They listed the yield strength, tensile strength, elongation and modulus of elasticity for Ti–6Al–V Christensen et al. (2007a, 2008) made Ti–6Al–4V ELI specimens using the EBM equipment with some changes in the fabrication parameters. They examined microstructures and reported the mechanical properties with the data of the fatigue resistance. Some of their specimens were treated using the HIP process. They made tensile specimens by machining the EBM rods. Their group has another report of the mechanical test data of Ti–6Al–4V ELI fabricated using the Arcam® equipment (Christensen, 2007). They examined the effect of the HIP treatment and again used the machined tensile bars. There is compiled data reported in 2007 from Arcam® AB (Sweden) about the properties evaluation of Ti–Al–4V ELI fabricated by their equipment (Arcam® A2). They used the EBM specimens machined for the tensile test. In 2009, Murr et al. published articles (Murr et al., 2009a,b) of detailed examination of microstructures and mechanical properties of the Ti–6Al–4V prepared using the Arcam® equipment (Arcam® EBM S400, Sweden). Their tensile specimens were also machined from the EBM fabricated rods. Prior to the present study, the tensile properties of Ti–6Al–4V ELI specimen made by the Arcam® equipment (Arcam® A2) were evaluated using the specimens with a larger dimension than those presently used (Chahine et al., 2008). The tensile data were obtained using machined and polished EBM specimens and also the EBM as-fabricated specimens with rippled surfaces. In Table 1, the mechanical properties published at various institutions and universities for some of the EBM- and SLM-fabricated Ti–6Al–4V or Ti–6Al–4V ELI are summarized.

As for data about fatigue characteristics of specimens manufactured using SLM or EBM, unlike more abundant tensile data, published values determined are limited. The data of titanium specimens prepared using SLM were reported by Santos et al. (2004) and Laoui et al. (2006). The results of the torsional fatigue test for the SLM pure titanium had the fatigue life of 10^6 cycles at the 80 MPa stress (Santos et al., 2004). Similar results were reported later from the same lab (Laoui et al., 2006). On the other hand, for the EBM titanium alloys (Ti–6Al–4V ELI), a report by Christensen et al. (2008) had an estimation of 10^7 cycle fatigue limit just below 594 MPa. A report from Arcam AB® (Thundal, 2008) also indicated that the fatigue life of EBM Ti–6Al–4V to be in the level of 10^7 cycles at 600 MPa.

In dentistry, from the standpoint of cost effectiveness, the cast prosthesis are often preferred to be used in the "as-fabricated" condition without any additional treatment after initial fabrication. Thus, in order to find the capability of the EBM process to fabricate acceptable dental prostheses of titanium alloys, the present study was started to examine not only their mechanical properties of as-fabricated EBM Ti–6Al–4V ELI specimens but also some other relevant characteristics including surface quality, microstructures, grindability and corrosion behaviors.

Table 1
Comparison of the mechanical properties published for some of the EBM- and SLM-fabricated Ti–6Al–4 or Ti–6Al–4V ELI.

	YS (MPa)	TS (MPa)	El (%)	*E* (GPa)	Remarks
EBM					
Lindhe and Harrysson (2003) Ti–6Al–4V	880	930	>10	128	Used HIP-specimen (likely machined)
Schroeder (2006) Ti–6Al–4V	910–960	950–1030	12–16	120	Used machined/polished specimens
Thundal (2008) Ti–6Al–4V	950	1020	14	114	
Christensen (2007) Ti–6Al–4V ELI	820	913	17	–	
Christensen et al. (2007b, 2008) Ti–6Al–4V ELI	800	876	16	–	Used HIP and machined specimens
	856	924	15	–	Used machined specimens
Chahine et al. (2008) Ti–6Al–4V ELI	–	1028	14	–	Used machined and polished tensile specimens
		928	3		Used as-fabricated specimens
Murr et al. (2009b) Ti–6Al–4V	1130	1180	>20	–	Used machined but unpolished specimens
Al-Bermani et al. (2010) Ti–6Al–4V	884–939	994–1031	12–14	–	
	841–875	939–978	13–14	–	
Koike and Okabe (2010) Ti–6Al–4V ELI	735	775	2.3	93	Used as-fabricated specimens
SLM					
Das et al. (1998) Ti–6Al–4V SLS/HIP	–	1117	5	–	Used machined/polished specimens
Lü et al. (2001) Ti–6Al–4V SLS/HIP Same as Santos	885	962	23	110	Used machined/polished specimens
Levy et al. (2003) Ti–6Al–4V SLS/HIP	–	1200–1400	1–2	–	Used machined/polished specimens
Murr et al. (2009b)	1350	1450	0.5	128	Used machined specimens

2. Materials and methods

2.1. Electron beam melting (EBM) system

The most current model of the EBM system is the Arcam® A2 by Arcam® AB in Sweden. Currently, the Arcam® A2 equipment is available at several universities and institutions in the United States. There are also companies that have the equipment. Generically, this free-form, rapid manufacturing machine is often called an electron beam melting (EBM), although selective electron beam melting (SEBM) is a much more descriptive notation when considering its fabrication mechanism. Detailed descriptions about the principles of the EBM system and the operating conditions of preparing specimens are given elsewhere (Chahine et al., 2008).

A schematic drawing of the Arcam® A2 EBM equipment is shown in Fig. 1. It consists of the electron beam gun compartment and the specimen-fabrication compartment. In order to use a high-quality electron beam, the electron beam gun compartment is kept in the vacuum at 7.5×10^{-7} Torr. On the other hand, the specimen-fabrication compartment is kept in the vacuum at 7.5×10^{-5} Torr to reduce oxidation and contamination of titanium specimens. Since the use of a vacuum is a necessity for a quality electron beam, this equipment is ideal for fabricating titanium components which are easily oxidized in air. The specimen compartment houses the powder hoppers to supply the metal powder and the rake or power distributor to spread the powder during the layering process on a build table, on which a designed object or component are built up layer by layer.

The fabrication of a 3D object goes through several stages as shown in Fig. 2. At first, a CAD model of the object is produced into data formatted in stl. using a digital file obtained by computer tomography (CT scan) of the original object. The EBM equipment builds a metal powder layer which is spread each time at a thickness of approximately 100 μm thick, from the bottom up, by selectively scanning the focused electron beam first, to preheat or sinter specific areas of the metal powder layer as directed by the 3D CAD model. The purpose of the pre-heating process at lower beam power is to lightly sinter the powder to prevent the metal powder from spreading. Then, the same selected areas are melted using full beam power, resulting in the formation of a molten pool and solidifying it into a fully dense layer with a fine-scale microstructure. The table is then lowered, and a new powder layer is spread to continue building the 3D object. These three basic processes, powder spreading, pre-heating, and melting, are repeated until the 3D object is

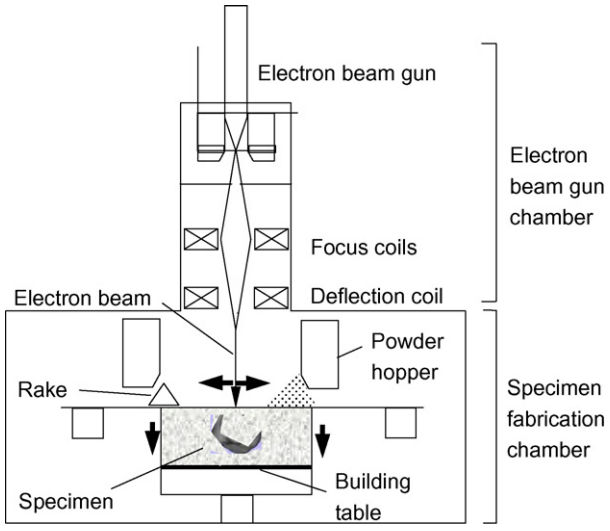

Fig. 1. Schematic drawing of an electron beam melting system.

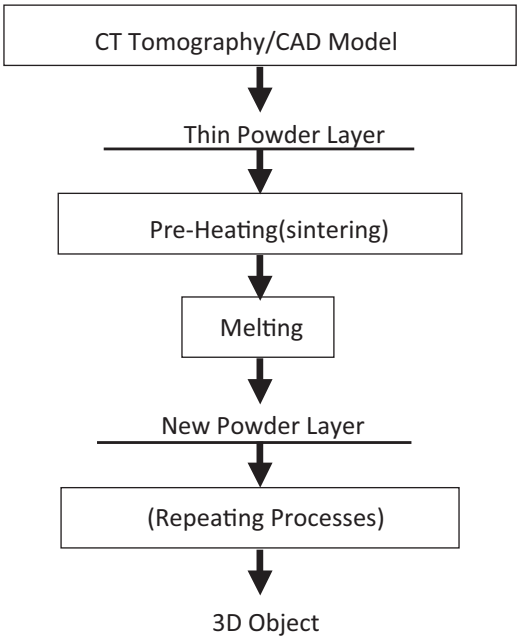

Fig. 2. Flow sheet of fabricating 3D object using EBM.

completely fabricated according to the design. The machine has a building speed of 6–7 mm/h, and the entire build occurs in the vacuum environment. Thus, a 6 mm – high product can be directly built from a CT file within 1 h (Chahine et al., 2008).

2.2. Fabrication of specimens

Using the Ti–6Al–4V ELI powder (ASTM Grade 23, Arcam® AB), three types of specimens, dumbbell-shaped specimens (20 mm gauge length, 3 mm diameter) for the tensile testing; and two kinds of plate specimens (10 mm × 10 mm × 2 mm or 30 mm × 30 mm × 4 mm) for metallography, the evaluation of corrosion behavior and grindability, were fabricated in the Arcam® A2 EBM system. The Ti–6Al–4V ELI powder used consisted of the spherical particles with the average particle size of 40 μm. The operational parameters used in the process of fabricating specimens were the same as used in the previous study (Chahine et al., 2008). Specimens were directly fabricated into dumbbell shapes by EBM as designed in stl. files. The tensile dumbbell specimens (20 mm gauge length, 3 mm diameter) were prepared the electron beam direction parallel to the long axis of the specimens. On the other hand, plate specimens were made by building so that the square surfaces were built perpendicular to the direction of the electron beam. In addition, the dumbbell specimens and two types of plate specimens (10 mm × 10 mm × 2 mm or 3.5 mm × 8.5 mm × 30.5 mm) were cast with commercially pure titanium (CP Ti, ASTM Grade 2, Titanium Industry, TX, USA) or Ti–6Al–4V ELI (ASTM Grade 23, Titanium Industry) in a MgO-based mold (Selevest CB, Selec, Japan) using a centrifugal casting machine (Ticast Super R, Selec) specifically designed for dental titanium casting. Detailed procedures of casting titanium are given elsewhere (Koike et al., 2007). These cast specimens were used as controls. The internal porosity of each of the specimens was examined with a conventional dental X-ray unit (Siemens 5938303, Munich, Germany) under the following conditions: target film distance, 50 cm; tube voltage, 70 kVp; tube current, 15 mA; exposure, 1–2 s. Specimens with noticeably large pores were excluded from further testing. The minimum diameter of pores detected by this method was estimated to be 0.05 mm (Koike et al., 2005). Prior to tensile testing, each cast specimen was examined with X-ray radiography to ensure their structural soundness; specimens with pores larger than 0.05 mm were excluded. Also, wrought Ti–6Al–4V ELI (grade 23, Titanium Industry) in a plate form (50 mm × 50 mm × 4 mm) was obtained and used for each property evaluation excluding the tensile testing. The wrought Ti–6Al–4V ELI plates were air-cooled after heating at 1300 °F (704 °C) for 1 h.

2.3. Metallography

Pieces (10 mm × 10 mm × 2 mm, $n = 2$) of each metal were metallographically polished and etched using a hydrofluoric acid-based solution (ASM Handbook Committee, 1985). The prepared surfaces were examined using an optical microscope (Epiphot 200, Nikon, Japan) and a scanning electron microscope (SEM) (JSM-6300, JEOL, Tokyo, Japan) equipped with an energy dispersive spectroscope (EDS) analysis system using a Si (Li) X-ray detector (Noran Instruments, Middleton, WI, USA). For the EBM specimens, planes both parallel and perpendicular to the beam direction were examined.

2.4. Mechanical properties

Tensile testing ($n = 4$) was performed using the dumbbell-shaped specimens (both the EBM fabricated and cast CP Ti and Ti–6Al–4V ELI specimens) at a crosshead speed of 0.25 mm/min at room temperature. Yield strength at 0.2% offset (YS), ultimate tensile strength (TS), modulus of elasticity (E) and percent elongation (El) were determined. Typical testing processes employed are given in an earlier report (Koike et al., 2005).

2.5. Hardness testing

The Vickers microhardness was determined with a 200 g load and 15 s dwell time at more than 300 μm below the surface using a microhardness tester (FM-7, Future Tech, Tokyo, Japan). The microhardness of four randomly chosen areas was determined on two specimens for each metal ($n = 8$). The experimental procedures for each phase of testing are given elsewhere (Koike et al., 2005).

2.6. Grindability

Larger plate specimens (30 mm × 30 mm × 4 mm,) were cut into rectangular shapes of 8 mm × 30 mm by slicing them parallel to the direction of the electron beam of the EBM system, which is perpendicular to the plane of the stacking layers. Both surfaces of the 8 mm × 30 mm plate were ground 0.5 mm so that the resultant thickness of the specimens was reduced to 3 mm. On the other hand, all the cast specimens were ground from castings of 3.5 mm × 8.5 mm × 30.5 mm, so that the thickness after the removal of the α-case was 3 mm. In addition, specimens with the dimension similar to other grindability specimens were prepared using plates of wrought Ti–6Al–4V ELI and CP Ti (Titanium Industry). Grindability ($n = 8$) was evaluated as volume loss (mm^3) after abrasion for one minute, using a SiC wheel of specimens (13 mm diameter, 1.5 mm thick: 703-120, Brasseler USA, USA) applied 100 gf at 1250 m/min. The testing method used for this evaluation was similar to that in a previous study (Koike et al., 2005). One of the side walls of 30 mm × 3 mm of the specimens was placed perpendicular to the circumferential surface of the SiC wheel so that the direction of the grinding was parallel to the layer of the EBM specimen. The volume of metal ground, evaluated by a reduced weight of specimens, was used to compare the grindability among the various metals (Koike et al., 2007).

2.7. Corrosion behavior

The corrosion characteristics of various alloy specimens were evaluated using the electrolytic method and a potentiostatic polarization technique. Evaluation of the corrosion behavior was performed ($n = 4$, 10 mm × 10 mm × 2 mm) in a modified Tani-Zucchi synthetic saliva maintained at 37 °C as previously reported (Koike et al., 2003). The open circuit potential (OCP: V), polarization resistance (R_p: MΩ cm^2), corrosion current density (I_{corr}: A/cm^2) and passivation current density (I_{pass}: A/cm^2) were evaluated using a potentiostat (Model 273A; EG&G Princeton Applied Research, Princeton, NJ, USA). For the potentiodynamic corrosion tests, the open circuit potential was evaluated up to 16 h in the aerated electrolyte. Following the OCP measurement, determination of linear polarization and cathodic polarization were conducted in aerated conditions and anodic polarization in deaerated conditions over the ranges and scanning rate as previously reported (Koike et al., 2003). The polarization resistance (R_p), the cathodic Tafel slope (β_c: V/decade) and the anodic Tafel slope (β_a: V/decade) were calculated. Using these three calculated parameters, β_a, β_c and R_p, the corrosion current density, or I_{corr} (A/cm^2), was determined by using the Stern-Geary equation, $I_{corr} = \beta_a\beta_c/2.3R_p(\beta_a + \beta_c)$ (Stern and Geary, 1957). In addition, the passive current density, or I_{pass} (A/cm^2), at 500 mV and the breakdown potential E_b (V) (the potential where the current density noticeably increases with increasing potential) was determined. A summary of the experimental conditions is given in Table 2.

Table 2
Experimental conditions for determination of corrosion behavior.[a]

Method	Atmosphere	Potential range (mV)	Scan rate (mV/s)	Corrosion parameters
Open-circuit potential (OCP)				OCP: OCP (mV) 16 h
Linear polarization	(Aerated air + 10% CO_2)	−8 < Ocp to OCP < +8	0.1	Polarization resistance: R_p ($M\Omega\,cm^2$)
Potentiodynamic cathodic polarization		OCP to 300 < OCP	0.167	Cathodic Tafel slope: β_c (V/decade)
Potentiodynamic anodic polarization	(Deaerated N_2 + 10% CO_2)	200 < OCP to 2000 > OCP	0.167	Anodic Tafel slope: β_a (V/decade)
				Corrosion current density: I_{corr} (A/cm^2) $I_{corr} = \beta_a\beta_c/2.3R_p(\beta_a+\beta_c)$
				Passive current density at 500 mV: I_{pass}(A/cm^2)

[a] Saturated calomel electrode (SCE) was used as the reference electrode for all the measurements.

2.8. Statistical analysis

The results for all tests, except for corrosion testing, were analyzed using one-way ANOVA and the Tukey's test at $\alpha = 0.05$. The data for the corrosion tests were statistically analyzed by Kruskai–Walls H test at a significance level of $\alpha = 0.05$.

3. Results

3.1. Exterior appearance

Fig. 3 compares the external appearances of a plastic dumbbell pattern used as the template for preparing a mold for casting the tensile specimens, a cast Ti–6Al–4V ELI specimen and also an EBM-fabricated Ti–6Al–4V ELI specimen. The EBM specimen was made based on the dimensional information of the stl. file used in fabricating it in the EBM system. In Fig. 3, an enlarged view of the gauge section of the EBM dumbbell specimen is also included where a rippled, exterior appearance is seen.

3.2. Microstructure

Fig. 4a–d shows selected microstructures of a typical EBM-fabricated Ti–6Al–4V ELI (Fig. 4a), cast Ti–6Al–4V ELI (Fig. 4b), wrought Ti–6Al–4V ELI (Fig. 4c) and cast CP Ti (Fig. 4d), respectively. The microstructure of the EBM Ti–6Al–4V ELI was the one taken from the specimen surface perpendicular to the EBM build direction. The micrographs of an EBM and a wrought Ti–6Al–4V ELI (Figs. 4a and c) show their interior structure whereas the micrographs of a cast Ti–6Al–4V ELI and a CP Ti show microstructures near the cast surface (Fig. 4b and d). Except for the wrought specimens, the widmanstätten, basketweave microstructures of the α titanium platelets are seen, although their degree in the structural fineness is different among them. In the cast specimens, a typical α-case microstructure consisting of columnar α crystals are clearly seen in the CP Ti micrograph (Fig. 4d). On the other hand, no α-case was observed near the surface of the EBM-fabricated specimens. The microstructure of the wrought Ti–6Al–4V ELI (Fig. 4c) consisted of a slightly elongated α grains and intergranular β grains which is a typical microstructure for the heat treatment condition that the specimen received (ASM Handbook, 1985). The microstructural observation of the present EBM alloy specimens indicates that there existed no "discontinuous" microstructure and they appear to have sound, solid structure.

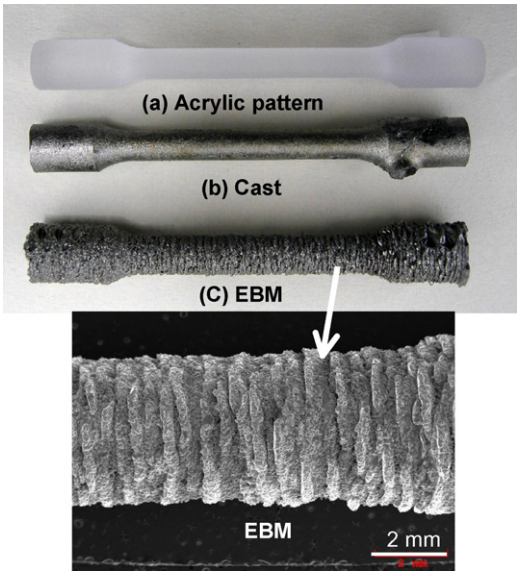

Fig. 3. Exterior appearance of (a) a plastic dumbbell pattern, (b) a cast Ti–6Al–4V ELI specimen and (c) an EBM specimen with an enlarged view of an EBM specimen.

3.3. Mechanical properties

Table 3 summarizes the tensile properties and microhardness of the specimens tested in our laboratory and reported data from the manufacturer (Titanium Industry) for the wrought Ti–6Al–4V ELI and CP Ti. The yield strength of the EBM Ti–6Al–4V ELI specimens is comparable to that of the cast specimens. However, the value is lower than that of the wrought specimens ($p < 0.05$). The tensile strength and ductility of the cast and wrought Ti–6Al–4V ELI specimens were higher than those of the EBM Ti–6Al–4V ELI specimens ($p < 0.05$). On the other hand, the Vickers microhardness of the EBM Ti–6Al–4V ELI specimens was higher than that of the cast and wrought Ti–6Al–4V ELI specimens ($p < 0.05$).

3.4. Grindability

The results of the grindability test are summarized in Table 4. Among all the specimens evaluated, the grindability of the EBM Ti–6Al–4V ELI was significantly higher than that of all the other alloy specimens including CP Ti used in the present study ($p < 0.05$). The results are consistent with our previous findings (Okabe et al., 2004; Chan et al., 2006) that the grindability of titanium alloys is negatively correlated with the ductility.

3.5. Corrosion behavior

The results of the corrosion parameters determined are summarized in Table 5. Among the determined parameters, the statistical differences were found in the polarization resistance (R_p: $p = 0.05$), the corrosion current density (I_{corr}: $p = 0.03$) and the passive current density (I_{pass}: $p = 0.36$). As expected, the CP titanium specimen exhibited the better corrosion behavior compared to Ti–6Al–4V ELI specimens. No significant differences were seen in all the param-

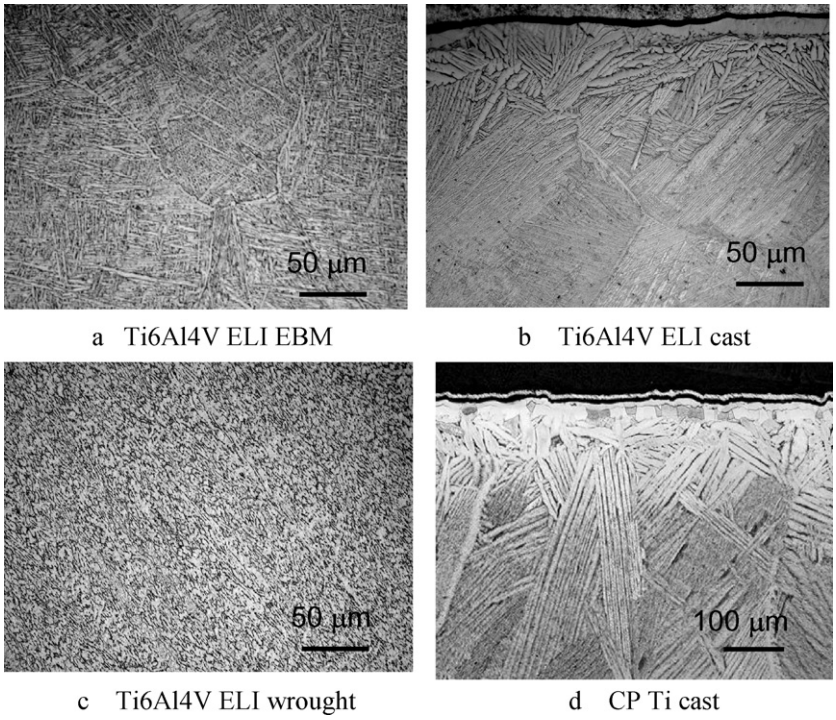

Fig. 4. Optical micrographs of alloys used: EBM Ti–6Al–4V ELI. Wrought Ti–6Al–4V ELI. Cast Ti–6Al–4V ELI. Cast CP Ti.

Table 3
Mechanical properties of specimens tested.

Specimen	YS (MPa)	TS (MPa)	El (%)	*E* (GPa)	HV
Ti–6Al–4V ELI (EBM)	735 (28)[c]	775 (26)[e]	2.3 (0.8)[d]	93 (2)[b]	369 (2)[c]
Ti–6Al–4V ELI (wrought)	860 (14)[d]	931 (21)[d]	14 (3.7)[b]	–	327 (1)[b]
Ti–6Al–4V ELI (cast)	734 (8)[c]	851 (23)[c]	4.4 (0.7)[d]	102 (1)[a]	333 (9)[b]
CP Ti (wrought)	335 (31)[a]	474 (9)[a]	29 (0.5)[a]	–	184 (4)[a]
CP Ti (cast)	463 (32)[b]	555 (27)[b]	8.7 (0.7)[c]	106 (1)[a]	185 (13)[a]

Values are means (SD) for properties of tested alloys. Identical letters indicate no statistical differences ($p > 0.05$). The yield strength, tensile strength and elongation data of wrought metals were from a data sheet of the manufacturer (Titanium Industry).

Table 4
Grindability of specimens tested.

Alloy	Ti–6Al–4V ELI (EBM)	Ti–6Al–4V ELI (wrought)	Ti–6Al–4V ELI (cast)	CP Ti (wrought)	CP Ti (cast)
Grindability (mm^3)	2.45 (0.41)[a]	1.90 (0.12)[b]	1.99 (0.18)[b]	1.11 (0.20)[c]	1.17 (0.41)[c]

Values are means (SD) for properties of tested alloys. Identical letters indicate no statistical differences ($p > 0.05$).

eters between the EBM Ti–6Al–4V specimens, wrought Ti–6Al–4V specimens and cast Ti–6Al–4V ELI specimens.

4. Discussion

In the present study, the microstructures and mechanical properties along with grindability and corrosion behavior of the Ti–6Al–4V ELI specimens were investigated. The Ti–6Al–4V ELI specimens were prepared using a newly introduced rapid prototyping machine, an electron beam melting (EBM) equipment, Arcam® A2 (Arcam® AB, Sweden). The tensile data of the EBM fabricated specimens were compared with those of wrought and cast Ti–6Al–4V ELI. The data for the wrought alloy was obtained from the manufacturer whereas those of the cast alloy were obtained in our laboratory (Koike and Okabe, 2010). As described in Section 1, a number of investigators examined the mechanical properties of the EBM- and the SLM-fabricated Ti–6Al–4V ELI or Ti–6Al–4V specimens. Their yield strength, tensile strength and

Table 5
Corrosion characteristics of metals tested.

Specimen	OCP (mV)	R_p ($M\Omega\,cm^2$)	I_{corr} (nA/cm^2)	I_{pass} (nA/cm^2)
Ti–6Al–4V ELI (EBM)	−246 (81)[a]	0.45 (0.27)[a]	199 (90)[a]	1644 (583)[a]
Ti–6Al–4V ELI (wrought)	−158 (15)[a]	1.36 (0.48)[ab]	49 (25)[ab]	837 (249)[ab]
Ti–6Al–4V ELI (cast)	−246 (66)[a]	0.75 (0.71)[ab]	198 (158)[a]	1137 (752)[ab]
CP Ti (wrought)	−239 (52)[a]	2.46 (0.10)[bc]	16 (10)[b]	551 (113)[b]
CP Ti (cast)	−300 (71)[a]	3.99 (0.82)[c]	9 (2)[b]	747 (60)[b]

Values are means (SD) for parameters of tested alloys. Identical letters indicate no statistical differences ($p > 0.05$).

Table 6
Oxygen content (wt%) in various Ti–6Al–4V ELI specimens including the Ti–6Al–4V ELI powders.

	Oxygen (wt%)
Arcam® alloy powder	0.120[a]
Arcam® alloy powder (recycled)	0.34 ± 0.01[b]
EBM specimen	0.31 ± 0.01[b]
Cast specimen	0.22 ± 0.00[b]
Wrought specimen[c]	0.110

[a] Nominal composition obtained from the powder manufacturer (Arcam®).
[b] Analyzed values obtained using an infrared adsorption spectroscope.
[c] Nominal composition obtained from the alloy manufacture (Titanium Industry).

elongation determined at different experimental sites, together with their modulus of elasticity (only few reported) are summarized in Table 1. Our tensile data of the EBM Ti–6Al–4V ELI are inferior to many of the corresponding values reported by other institutions. The main reason is that our dumbbell specimens used were in an as-fabricated condition. No specific surface modifications were made before the tensile test. Our specimens were directly fabricated into dumbbell shapes by EBM as designed in stl. file. As seen in Fig. 3, the surface roughness in the gauge length of our EBM dumbbell specimens was found much rougher than that of the cast specimens. Also, note that specimens used in the determinations of the tensile properties at other institutions were all machined and some are even polished. Our EBM as-fabricated specimens had rough, rippled surfaces. The large stress concentrations caused by the rippled surface permit crack extension at lower applied stresses than required to initiate a crack in smooth tensile specimens. The elongation of the present EBM specimens (2.3%) was much lower than that of the reported data in most of the EBM specimens of other institutions (16 and 25%) and also lower when compared to the elongation of the cast specimen (4.4%). Earlier, the tensile tests of the EBM specimens were performed with two different surface conditions. One of the groups was EMB as-fabricated dumbbell specimens conformed to ASM E8 standard and the other one was the specimens machined using a water-jet cutting and polished using 400 μm sandpaper (Chahine et al., 2008). The tensile strength and elongation of machined and as-fabricated specimens were 1028 MPa and 3%, and 928 MPa and 14%, respectively. As expected, this result clearly indicated the effect of the surface quality on the strength and elongation. Yield strength and tensile strength of the present EBM specimens without any surface improvements were similar to each other and near 750 MPa, whereas the reported tensile strength data of machined test bars are higher than 1000 MPa.

The low elongation of the present as-fabricated EBM Ti–6Al–4V ELI specimens was thought to be influenced by the oxygen content in addition to the rippled surfaces as mentioned above. The oxygen content of the specimens fabricated by EBM was thought to have been affected by the oxygen content in the alloy powder used to prepare them. Thus, using an infrared adsorption spectroscopic analyzer, the oxygen content was determined for the Arcam® AB Ti–6Al–4V ELI alloy powder in the same batch that was used to fabricate specimens along with the oxygen contents in the EBM specimens made from that powder. That powder was the one recycled several times before the present specimens were made. The values of the oxygen content are listed in Table 6. The table lists the oxygen contents determined in two different alloy powders, the powder as delivered from the alloy manufacturer, Arcam® AB, and the recycled powder that was used for the present study. In addition, Table 6 includes the oxygen content in the Ti–6Al–4V ELI cast in our laboratory and wrought Ti–6Al–4V ELI delivered from the manufacturer. A high oxygen content in the present EBM specimens (0.31%) was the result of using recycled alloy powders whose oxygen content was near 0.34%. The oxygen content in the tensile

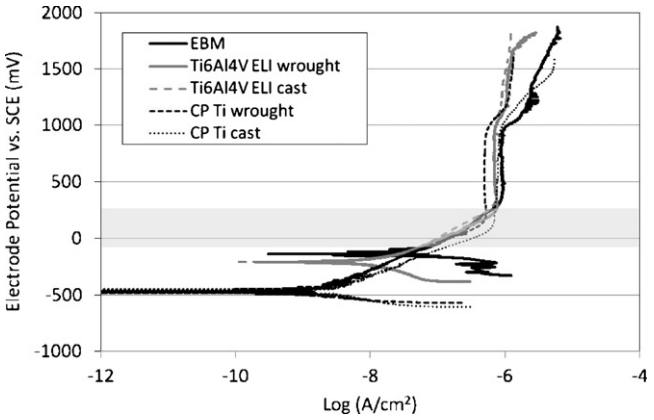

Fig. 5. Typical anodic polarization curves for the metals used.

specimens reported from some institutions is at most 0.25% (Das et al., 1998; Al-Bermani et al., 2010). The oxygen content in the cast and wrought specimens determined were 0.22% and 0.11%, respectively (Koike and Okabe, 2010). In general, the oxygen contents in the titanium and its ductility and the strengths [thus, the hardness (Ashby and Jones, 1980)] are negatively correlated (Jaffee, 1958; Collings, 1984). Williams et al. (1972) explained that an increase of the oxygen content in α titanium increases the tendency for slip localization and the formation of planar slip bands. The low elongation found for the EBM specimen was probably due to its high oxygen content and the rippled surfaces of the test specimens. This explanation can be extended to describe a similar phenomenon to titanium alloys (Donachie, 2000).

As for the hardness a higher value of the EBM specimens, it is believed to be due probably to the reduced a colony size.

The low ductility leads to an excellent grindability of the EBM specimens which is favorably accepted for the dental applications. The grindability of the present EBM Ti–6Al–4V ELI when compared to either the cast or wrought corresponding alloy specimens (Koike et al., 2007) was significantly better (Table 4). Also note that the present grindability is uncomparably better to that of CP Ti. An outstanding present grindability is due to its low ductility, which is consistent with our theorized explanation of the grindability and ductility of titanium alloys (Chan et al., 2006).

As listed in Table 5 of the corrosion data of different CP Ti and Ti–6Al–4V ELI specimens, a majority of the evaluated corrosion properties for the CP Ti specimens, both wrought and cast, indicated a better corrosion behavior than that for all the present Ti–6Al–4V ELI specimens. This is because the addition of alloying elements changes in anodic dissolution kinetics of the solute elements, affects local action cells and changes in the behavior of grain boundary attack (Scully, 1975). A less corrosion resistance of the Ti–6Al–4V ELI can be explained as the compositional difference between the α and β plates which result in the formation of a galvanic potential at the grain boundary. Within the range of the electrode potential employed, any significant differences in the electrochemical behavior in an artificial saliva were found among all the Ti–6Al–4V ELI alloy specimens made by different fabrication methods. The present EBM Ti–6Al–4V ELI specimens exhibited an excellent passivation and corrosion characteristics in the oxidation potential range [(−58 mV to 212 mV vs. saturated calomel electrode (SCE)] of the normal human oral cavity (see shaded area of Fig. 5) (Ewers and Greener, 1985).

One unique feature of the EBM fabricated specimens is their unusual surface appearance when contrasted to that of specimens produced by common methods such as casting, forging, rolling and machining. In Fig. 4, exterior appearances of a Ti–6Al–4V ELI specimen fabricated by EBM process and made by casting are compared.

The surface of the EBM specimens are covered by rippled layers with some unused alloy particles bonded on it (Fig. 4c). This surface is the result of the EBM fabrication process which repeatedly sinters and melts the alloy powder layers of 100–150 μm. On the other hand, the exterior surfaces of cast specimens (Fig. 4b) are much smoother. Note that both specimens were the as-fabricated condition in each fabricating method. The as-fabricated rippled surfaces of EBM processed alloy may be useful for some dental applications where an irregular surface is beneficial.

5. Conclusion

(1) Tensile dumbbell specimens of Ti–6Al–4V ELI were directly prepared in Arcam® A2 electron beam melting (EBM) system using a stl. file of the designed shape for needed specimens. Specimens fabricated had a sound/solid α/β lamelar microstructure with a rippled surface.
(2) The yield strength and tensile strength of the EBM specimens were 735 and 775 MPa, respectively. The elongation was 2.4%. These values were comparable to those of cast Ti–6Al–4V ELI. The cast specimens exhibited slightly higher tensile strength (860 vs. 735 MPa) and elongation (4.4 vs. 2.3%). These differences were thought to be due to rippled, rough specimen surfaces and higher oxygen content in the EBM specimens (0.34 vs. 0.22%). A higher microhardness of the EBM specimens was probably due to their finer α/β lamellar microstructures.
(3) The grindability of the present EBM Ti–6Al–4V ELI specimens was much better than that of the wrought or cast specimens. The lower ductility of the EBM specimens appears to be responsible of a better grindability.
(4) The corrosion behavior in an artificial saliva of the Ti–6Al–4V ELI specimens fabricated by three different methods (EBM, cast and wrought) were comparable to each other. Although the CP Ti specimens (cast and wrought) showed less electrochemical activity than that of the Ti–6Al–4V ELI over the tested potential ranges, the present Ti–6Al–4V ELI exhibited an outstanding passivation and corrosion characteristics in the oxidation potential ranges of the normal human potential range.
(5) The mechanical properties and corrosion characteristics of the present Ti–6Al–4V ELI fabricated by the EBM process are well within those of the presently used precious and non-precious dental casting alloys (Koike et al., 2007). A unique, rippled surface of the as-fabricated EBM alloys may find some applications in dentistry.

Acknowledgements

This study was partially funded by the Baylor Oral Health Foundation. The Authors gratefully acknowledge Dr. Hideki Fujii, Nippon Steel Corp., Chiba Japan, for analyzing the oxygen content of the specimens.

References

Al-Bermani, S.S., Blackmore, M.L., Zhang, W., Todd, I., 2010. The origin of microstructural diversity, texture, and mechanical properties in electron beam melted Ti–6Al–4V. Metall. Trans. Phys. Metall. Mater. 41, 3422–3434.
Anusavice, K.J., 2003. Phillips' Science of Dental Materials, 11th ed. Saunders, St. Louis, MO.
Ashby, M.F., Jones, D.R.H., 1980. Engineering materials. In: An Introduction to Their Properties and Applications. Pergamon Press, Oxford.
ASM Handbook Committee, 1985. Metals Handbook. Metallography and Microstructures, vol. 9., 9th ed. American Society for Metals, Metals Park, OH.
Bertol, L.S., Júnior, W.K., Silva, F.P.D., Aumund-Kopp, C., 2010. Medical design: direct metal laser sintering of Ti–6Al–4V. Mater. Des. 31, 3982–3988.
Chahine, G., Koike, M., Okabe, T., Smith, P., Kovacevic, R., 2008. The design and production of Ti–6Al–4V ELI customized dental implants. JOM 60, 50–55.
Chan, K.S., Koike, M., Okabe, T., 2006. Grindability of Ti alloys. Metall. Mater. Trans. A 87, 1323–1331.
Christensen, A., 2007. Additive manufacturing in metal: new option for medical applications. In: Moldmarking Technology, Design, Build, Manage Magazine. Medical Modeling. The Tactile imaging Solutions Company.
Christensen, A., Lippincott, A., Kircher, R., 2007a. Qualification of Electron Beam Melted (EBM) Ti6AI4V-ELI for orthopaedic implant applications. In: Medical Modeling. L.L.C. Golden, CO, pp. 1–7.
Christensen, A., Lippincott, A., Kircher, R., 2007b. An Introduction to Electron Beam Melting with Ti6Al4V-ELI for the Orthopaedic Device Industry. Spring, BONE-Zone, pp.14–17.
Christensen, A., Kircher, R., Lippincott, A., 2008. Qualification of Electron Beam Melted (EBM) Ti6AI4V-ELI for orthopaedic applications. In: Medical Device Materials IV: Proceedings of the Materials and Processes for Medical Devices Conference , pp. 48–53.
Collings, E.W., 1984. The Physical Metallurgy of Titanium Alloys. American Society for Metals, Metals Park, OH.
Cooper, K.P., 2001. Building components by laser-additive processing. JOM 53, 29.
Das, S., Wohlert, M., Beaman, J.J., Bourell, D.L., 1998. Producing metal parts with selective laser sintering/hot isostatic pressing. JOM 50, 17–20.
Das, S., 2003. Physical aspects of process control in selective laser sintering of metals. Adv. Eng. Mater. 5, 701–711.
Donachie Jr., M.J., 2000. Titanium: A Technical Guide. ASM International, Materials Park, OH.
España, F.A., Balla, V.K., Bandyopadhyay, A., 2010. Laser surface modification of AISI 410 stainless steel with brass for enhanced thermal properties. Surf. Coat. Technol. 204, 2510–2517.
Ewers, G.J., Greener, E.H., 1985. The electrochemical activity of the oral cavity. J. Oral Rehabil. 12, 469–476.
Harrysson, O.L., 2005. Direct fabrication of custom orthopedic implants using electron beam melting technology. In: Gibson, I. (Ed.), Advanced Manufacturing Technology for Medical Applications; Reverse Engineering, Software Conversion and Rapid Prototyping. John Wiley & Sons, Ltd..
Harrysson, O.L., Cansizoglu, O., Marcellin-Little, D.J., Cormier, D.R., West II, H.A., 2008. Direct metal fabrication of titanium implants with tailored materials and mechanical properties using electron beam melting technology. Mater. Sci. Eng. C 28, 366–373.
Haslauer, C.M., Springer, J.C., Harrysson, O.L.A., Loboa, E.G., Monteiro-Riviere, N.A., Marcellin-Little, D.J., 2010. In vitro biocompatibility of titanium alloy discs made using direct metal fabrication. Med. Eng. Phys. 32, 645–652.
Heinl, P., Korner, C., Singer, R.F., 2008. Selective electron beam melting of cellular titanium: mechanical properties. Adv. Eng. Mater. 10, 882–888.
Hollister, S.J., Lin, C.Y., Saito, E., Lin, C.Y., Schek, R.D., Taboas, J.M., Williams, J.M., Partee, B., Flanagan, C.L., Diggs, A., Wilke, E.N., Van Lenthe, G.H., Müller, R., Wirtz, T., Das, S., Feinberg, S.E., Krebsbach, P.H., 2005. Engineering craniofacial scaffolds. Orthod. Craniofac. Res. 8, 162–173.
Jaffee, R.I., 1958. The physical metallurgy of titanium alloys. In: Chalmers, B. (Ed.), Progress in Metal Physics, vol. 7. Pergamon Press, London, pp. 65–163.
Khouja, N., Chu, T., Chahine, G., Kovacevic, R., Koike, M., Okabe, T., 2010a. In vivo evaluation of novel experimental implants. J. Dent. Res. 89 (Spec Iss A), 1103.
Khouja, N., Chu, T., Chahine, G., Kovacevic, R., Koike, M., Okabe, T., 2010b. In vivo evaluation of novel custom-made press-fit implants. J. Dent. Res. 89 (Spec Iss B), 1662.
Koike, M., Cai, Z., Fujii, H., Brezner, M., Okabe, T., 2003. Corrosion behavior of cast titanium with reduced surface reaction layer made by a face-coating method. Biomaterials 24, 4541–4549.
Koike, M., Ohkubo, C., Sato, H., Fujii, H., Okabe, T., 2005. Evaluation of cast Ti–Fe–O–N alloys for dental applications. Mater. Sci. Eng. C 25, 349–356.
Koike, M., Chan, K.S., Okabe, T., 2007. Dental Titanium Casting at Baylor College of Dentistry – Update. The Minerals, Metals and Materials Society, pp. 199–208.
Koike, M., Okabe, T., 2010. Titanium fabricated by electron beam melting for dental applications. Shika. Zairyo. Kikai. 29, 61–67.
Kotila, J., Syvänen, T., Hänninen, J., Latikka, M., Nyrhilä, O., 2007. Direct metal laser sintering – new possibilities in biomedical part manufacturing. Mater. Sci. Forum. 534–536, 461–464, PART 1.
Krishna, B.V., Bose, S., Bandyopadhyay, A., 2007. Laser processing of net-shape NiTi shape memory alloy. Metall. Trans. Phys. Metall. Mater. 38, 1096–1103.
Laoui, T., Santos, E., Osakada, K., Shiomi, M., Morita, M., Shaik, S.K., Tolochko, N.K., Abe, F., Takahashi, M., 2006. Properties of titanium dental implant models made by laser processing Proc IME C. J. Mech. Eng. Sci. 220, 857–863.
Levy, G.N., Schindel, R., Kruth, J.P., 2003. Rapid manufacturing and rapid tooling with layer manufacturing (LM) technologies, state of the art and future perspectives. CIRP Ann. – Manufact. Technol. 52, 589–609.
Li, X., Wang, C., Zhang, W., Li, Y., 2009. Fabrication and characterization of porous Ti6Al4V parts for biomedical applications using electron beam melting process. Mater. Lett. 63, 403–405.
Lindhe, U., Harrysson, O.L., 2003. Rapid manufacturing with electron beam melting (EBM) – a manufacturing revolution? In: Solid Freeform Fabrication Symposium Proceedings , pp. 433–438.
Lü, L., Fuh, J.Y.H., Wong, Y.S., 2001. Laser-induced Materials and Processes for Rapid Prototyping. Kluwer Academic Publishers, Boston.
Mangano, C., Piattelli, A., d'Avila, S., Iezzi, G., Mangano, F., Onuma, T., Shibli, J.A., 2010a. Early human bone response to laser metal sintering surface topography: a histologic report. J. Oral. Implantol. 36, 91–96.
Mangano, C., Piattelli, A., Raspanti, M., Mangano, F., Cassoni, A., Iezzi, G., Shibli, J.A., 2010b. Scanning electron microscopy (SEM) and X-ray dispersive spectrometry

evaluation of direct laser metal sintering surface and human bone interface: a case series Lasers in Medical Science. Lasers Med. Sci. 28, 1–6.
Milberg, J., Sigl, M., 2008. Electron beam sintering of metal powder. Prod. Eng. 2, 117–122.
Mullen, L., Stamp, R.C., Brooks, W.K., Jones, E., Sutcliffe, C.J., 2009a. Selective laser melting: a regular unit cell approach for the manufacture of porous, titanium, bone in-growth constructs, suitable for orthopedic applications. J. Biomed. Mater. Res. B Appl. Biomater. 89, 325–334.
Mullen, L., Stamp, R.C., Fox, P., Jones, E., Ngo, C., Sutcliffe, C.J., 2009b. Selective laser melting: a unit cell approach for the manufacture of porous, titanium, bone in-growth constructs, suitable for orthopedic applications II. Randomized structures. J. Biomed. Mater. Res. B Appl. Biomater. 92, 178–188.
Murr, L.E., Esquivel, E.V., Quinones, S.A., Gaytan, S.M., Lopez, M.I., Martinez, E.Y., Medina, F., Hernandez, D.H., Martinez, E., Martinez, J.L., Stafford, S.W., Brown, D.K., Hoppe, T., Meyers, W., Lindhe, U., Wicker, R.B., 2009a. Microstructures and mechanical properties of electron beam-rapid manufactured Ti–6Al–4V biomedical prototypes compared to wrought Ti–6Al–4V. Mater. Charact. 60, 96–105.
Murr, L.E., Quinones, S.A., Gaytan, S.M., Lopez, M.I., Rodela, A., Martinez, E.Y., Hernandez, D.H., Martinez, E., Medina, F., Wicker, R.B., 2009b. Microstructure and mechanical behavior of Ti–6Al–4V produced by rapid-layer manufacturing, for biomedical applications. J. Mech. Behav. Biomed. Mater. 2, 20–32.
Okabe, T., Kikuchi, M., Ohkubo, C., Koike, M., Okuno, O., Oda, Y., 2004. Grindability and wear of titanium alloys. JOM 56, 46–48.
Ponader, S., Von Wilmowsky, C., Widenmayer, M., Lutz, R., Heinl, P., Körner, C., Singer, R.F., Nkenke, E., Neukam, F.W., Schlegel, K.A., 2010. In vivo performance of selective electron beam-melted Ti–6Al–4V structures. J. Biomed. Mater. Res. A Appl. Biomater. 92, 56–62.
Quante, K., Ludwig, K., Kern, M., 2008. Marginal and internal fit of metal-ceramic crowns fabricated with a new laser melting technology. Dent. Mater. 24, 1311–1315.
Regenfuss, P., Streek, A., Hartwig, L., Klötzer, S., Brabant, Th., Horn, M., Ebert, R., Exner, H., 2007. Principles of laser micro sintering. Rapid Prototyping J. 13, 204–212.
Santos, E.C., Osakada, K., Shiomi, M., Kitamura, Y., Abe, F., 2004. Fabrication of titanium dental implants by selective laser melting. Proc. SPIE – Int. Soc. Opt. Eng. 5662, 268–273.
Santos, E.C., Shiomi, M., Osakada, K., Laoui, T., 2006. Rapid manufacturing of metal components by laser forming. Int. J. Mach. Tool Manufact. 46, 1459–1468.
Schroeder, J.R., 2006. Advanced Manufacturing Technology Changes the Way Implants are Designed and Produced. Fall, BONEZone, pp. 17–20.
Scully, J.C., 1975. The Fundamentals of Corrosion. Pergamon Press, Oxford.
Stern, M., Geary, A.L., 1957. Electrochemical polarization. I. A theoretical analysis of the shape of polarization curves. J. Electrochem. Soc. 104, 46–63.
Thomsen, P., Malmstr, J., Emanuelsson, L., René, M., Snis, A., 2009. Electron beam-melted, free-form-fabricated titanium alloy implants: material surface characterization and early bone response in rabbits. J. Biomed. Mater. Res. B Appl. Biomater. 90, 35–44.
Thundal, S., 2008. Rapid manufacturing of orthopaedic implants. Adv. Mater. Process 166, 60–62.
Tolochko, N.K., Savich, V.V., Laoui, T., Froyen, L., Onifrio, G., signorelli, E., Titov, V.I., 2002. Dental root implants produced by the combined selective laser sintering/melting of titanium powders. Proc. IME J. Mater. Des. Appl. 216, 267–270.
Wehmöller, M., Warnke, P.H., Zilian, C., Eufinger, H., 2005. Implant design and production – a new approach by selective laser melting. Int. Congr. 1281, 690–695.
Williams, J.C., Sommer, A.W., Tung, P.P., 1972. Influence of oxygen concentration on the internal stress and dislocation arrangements in α titanium. Metall. Mater. Trans. B 3, 2979–2984.